LBL-34534
UC-401
Preprint

Lawrence Berkeley Laboratory
UNIVERSITY OF CALIFORNIA

CHEMICAL SCIENCES DIVISION

Submitted to Macromolecules

Pore-Size Distributions of Cationic Polyacrylamide Hydrogels Varying in Initial Monomer Concentration and Crosslinker/Monomer Ratio

M. Kremer, E. Pothmann, T. Rössler, J. Baker, A. Yee,
H. Blanch, and J. Prausnitz

August 1993

Prepared for the U.S. Department of Energy under Contract Number DE-AC03-76SF00098

DISCLAIMER

LBL-34534
UC-401

Pore-Size Distributions of Cationic Polyacrylamide Hydrogels Varying in Initial Monomer Concentration and Crosslinker/Monomer Ratio

Michael Kremer, Elmar Pothmann, Tobias Rössler, John Baker, April Yee, Harvey Blanch, and John Prausnitz

Department of Chemical Engineering
University of California

and

Chemical Sciences Division
Lawrence Berkeley Laboratory
University of California
Berkeley, CA 94720

August 1993

This work was supported by the Director, Office of Energy Research, Office of Basic Energy Sciences, Chemical Sciences Division of the U.S. Department of Energy under Contract Number DE-AC03-76SF00098 and by the National Institutes of Health under Grant No. R01GM46877-01.

Pore-Size Distributions of Cationic Polyacrylamide Hydrogels Varying in Initial Monomer Concentration and Crosslinker/Monomer Ratio

Michael Kremer, Elmar Pothmann, Tobias Rössler, John Baker, April Yee, Harvey Blanch, and John M. Prausnitz†

Chemical Engineering Department, University of California,
and
Chemical Sciences Division, Lawrence Berkeley Laboratory,
University of California
Berkeley, CA 94720

ABSTRACT: Pore-size distributions have been measured for cationic acrylamide-based hydrogels. We use the experimental mixed-solute-exclusion method, MSE, (introduced by Kuga) to obtain the solute-exclusion curve representing the amount of imbibed liquid inside the gel inaccessible for a solute of radius r. We use the Brownian-motion model (developed by Cassasa) to convert the size-exclusion curve into the pore-size distribution, which gives the frequency of pore radius R as a function of R. This theoretically-based interpretation of MSE data leads to the Fredholm integral equation that we solve numerically. Results are reported for a series of hydrogels containing acrylamide and 3% MAPTAC; the hydrogels differed in extent of crosslinking and/or initial concentration of monomer. Pore-size distributions shift to lower pore sizes with rising initial monomer concentration and with rising crosslinker-to-monomer ratio.

---

† To whom correspondence should be adressed

Introduction

Gels are cross-linked polymer networks swollen in a liquid medium. The imbibed liquid serves as a selective filter to allow free diffusion of some solute molecules, while the polymer network serves as a matrix to hold the liquid together. When the liquid is water, the cross-linked polymer is a hydrogel. Gels are well-known in foods and medicines, as absorbents in disposable diapers, as filters for water purification and as separation materials for chromatography and electrophoresis[1]. Gels are also of interest for controlled drug release[2] and for concentration of dilute solutions of macromolecules[3,4]. Despite much progress, fundamental understanding of gel properties is not yet sufficient for rational design of novel gel systems. For such designs, it is important to know how solute molecules interact with the gel, in particular, how they partition between the gel phase and the surrounding liquid phase. Partitioning depends on two major effects: size exclusion and molecular attraction/repulsion.

In this work we are concerned with the size-exclusion effect. Our goal is to determine pore-size distributions of some representative gels. For measuring gel microstructure, it is not possible to use common methods such as mercury porosimetry or nitrogen adsorption because gels are swollen in a liquid medium; therefore, pores are not readily accessible to mercury or nitrogen. Therefore, we use an indirect method for measuring pore-size distributions of gels based on the mixed-solute-exclusion (MSE) method introduced by Kuga[5,6]. This MSE method consists of three major steps:

- Solutions with dissolved solutes of known concentrations and molecular sizes are brought into contact with the swollen gel. The molecular sizes of the solutes must cover a substantial range. (These solutions are called stock solutions.)

- Diffusion of solutes into the gel until equilibrium is attained. Partitioning of a particular solute depends on both the size of the solute and on the size distribution of the gel pores.

- Separation of gel from its surrounding solution and subsequent concentration measurements of solutes in the equilibrated surrounding solution. The decrease of each solute concentration relative to its initial stock-solute concentration is used for calculating the gel's pore-size distribution.

To isolate the size-exclusion effect from the molecular attraction/repulsion effect, we performed experiments with solutes that do not have specific interactions with the charged-polymer matrix. To assure that size effects alone are responsible for the observed partitioning, in separate experimental studies we used two solute series: a poly - (ethylene glycol) / poly - (ethylene oxide) / ethylene oxide series, and a dextran / oligosaccharide series.

A polyelectrolyte hydrogel was prepared by aqueous free-radical reaction of acrylamide (AAm) copolymerized with the cationic (3-Methacrylamidopropyl) trimethylammonium chloride (MAPTAC)[7]. To obtain a network structure, N,N'-methylenebisacrylamide (BIS) was added as a crosslinking agent.

Pore-size distributions of polyelectrolyte hydrogels are strongly affected by three factors:

- Concentration of chemical crosslinks of polymer strands. That concentration is determined by the initial ratio of crosslinker to monomer.

- Concentration of physical entanglements of polymer strands. That concentration is determined by the inital concentration of all polymerizable monomers in aqueous solution.

- Net charge of the polyelectrolyte hydrogel. That charge is determined by initial concentration of cationic and/or anionic monomer.

These three factors can be quantified using the composition of the hydrogel, that is, by the nominal concentrations of monomer (AAm), co-monomer (MAPTAC) and cross-

linking agent (BIS) at preparation condition. The composition of a polyelectrolyte hydrogel is characterized by three concentration parameters:

$$\%C = \frac{\text{moles of BIS in feed solution}}{\text{total moles of monomer in feed solution}} \times 100$$

$$\%T = \frac{\text{mass of all monomers (g)}}{\text{volume of water (ml)}} \times 100$$

$$\%MAPTAC = \frac{\text{moles of MAPTAC in feed solution}}{\text{total moles of monomer in feed solution}} \times 100$$

The porous structure of a polyelectrolyte hydrogel is also affected by the properties of the surrounding solution, especially by dissolved ionic solutes (Donnan effect) and by dissolved uncharged solutes which partition unevenly between the gel phase and the solution phase (Osmotic effect).

Two series of hydrogels were prepared. In the first, %C varied (0.4 to 1.2%) while %T, %MAPTAC and the ionic strength of the solution were held constant (at 15%, 3% and 0.001 M, respectively). In the second, %T varied (15 to 30%) while %C, %MAPTAC and the ionic strength of the solution were held constant (at 0.2%, 15% and 0.001 M).

Theoretical Section

It is difficult to determine the porous structure of a swollen material because of its fragility. Hydrogels may consist of 90 or even 99 weight percent water and only 10 or 1 weight percent polymer network. The porous structure of a hydrogel exists only in contact with an aqueous solution; when dehydrated, the network collapses into a compact mass. Therefore, techniques for measuring the porous structure of a hydrogel must consider the polymer-aqueous solution interaction that is required to preserve the structure. Because displacement of the imbibed aqueous liquid with any other fluid (e.g., mercury, nitrogen) does not retain the original gel structure, classical porosity-measurement techniques such as mercury intrusion or gas adsorption cannot be used.

Optical methods such as scanning electron microscopy have been applied to determine the microstructure of hydrogels yielding a three-dimensional image of the structure. However, results from these methods strongly depend on the preparation technique of the hydrogel (e.g. critical-point drying with carbon dioxide, freeze-drying and freeze-etching). These preparation techniques modify the structure, sometimes shrinking hydrogels up to 20%, as observed using critical-point drying[8].

In the single-point solute exclusion method, introduced by Aggebrandt and Samuelson[9] to measure the pore structure of swollen cellulose, solutions containing one solute each are equilibrated with the material to be examined. Using this method, Stone et al[10-12] measured the pore structure of textile rayon and super tire cord using sugar and dextran probes. Kuga[5,6] introduced the mixed-solute-exclusion method utilizing one solution comprising all solute species together covering a wide molecular-weight range. For that case, concentration measurements of each solute must be preceded by a separation technique such as Gel Permeation Chromatography (GPC). Kuga investigated the porous structure of a cross-linked dextran gel (Sephadex) applying three different solute-exclusion methods. He performed his experiments using the above-mentioned single-point SE and mixed-SE and, in addition, the column solute-exclusion method. The latter is an inversion of GPC, where fully characterized polymer solutions are injected into a column packed with Sephadex. The elution behavior of the known polymer solutes is used to determine the pore structure. While this method saves much experimental time, it is applicable only to gel samples that are available as sufficiently rigid and finely divided particles such that their size and shape are independent of the surrounding liquid. It is therefore not useful for the hydrogels studied here.

Kuga's experimental results obtained with the single-point SE agree well with those obtained by the mixed-SE method. The column-SE method showed significant deviation in the high molecular-weight range, probably because of compression of gel particles during the packing procedure. For our purposes, the mixed-SE method is the best; it is

relatively fast and inexpensive. We use here a modified form of Kuga's mixed-SE method, as summarized below. Details are available elsewhere[13].

The initial total mass of the cationic hydrogel in the swollen state (m'_{GS}) [14]:ef.iscomposedthecross – linkedpolymernetwork(:f.m_{PN}), the imbibed liquid ($m'_{L,imb.}$) and possible excess liquid ($m_{L,exc.}$), which sticks to the surface of the hydrogel but does not contribute to the imbibed liquid:

$$m'_{GS} = m_{PN} + m'_{L,imb.} + m_{L,exc.} \quad . \tag{1}$$

Contacting the hydrogel with the stock solution causes a migration of solutes into the pores of the hydrogel. Due to the porous structure of the gel, the equilibrium concentrations of the solutes in the gel phase are smaller than those in the surrounding solution phase; this difference provides a driving force for the imbibed water to dilute the solution to achieve osmotic equilibrium. Therefore, the equilibrated total mass of the hydrogel is rewritten:

$$m''_{GS} = m_{PN} + m''_{L,imb.} \quad . \tag{2}$$

One part of the imbibed liquid is present in pores accessible to a solute of molecular weight M ($m''_{acc.}(M)$), while the remaining part is present in pores not accessible to this particular solute ($m''_{non-acc.}(M)$):

$$m''_{L,imb.} = m''_{acc.}(M) + m''_{non-acc.}(M) \quad . \tag{3}$$

The difference between the initial imbibed liquid ($m'_{Liq.,imb.}$) and the equilibrated imbibed liquid ($m''_{Liq.,imb.}$) represents the expelled water ($\Delta m_{expelled}$):

$$\Delta m_{expelled} = m'_{L,imb.} - m''_{L,imb.} \quad . \tag{4}$$

At the start of the experiment, the weight concentration of a solute of molecular weight M changes because the excess liquid ($m_{L,exc.}$), the expelled liquid ($m_{expelled}$) and the accessible part of the imbibed liquid ($m''_{L,acc.}$) contribute to a dilution of the surrounding solution:

$$w'(M) = \frac{m_{Solute}(M)}{\sum m_{Solutes} + m_{Solv.}} \sim \frac{m_{Solute}(M)}{m_{Solv.}} \quad (5)$$

$$w''(M) = \frac{m_{Solute}(M)}{m_{Solv.} + m''_{acc.}(M) + \Delta m_{expelled} + m_{L,exc.}} \quad . \quad (6)$$

The dilution ratio is defined as the concentration of the stock solution divided by the concentration at equilibrium:

$$\frac{w'(M)}{w''(M)} = \frac{m_{Solv.} + m''_{acc.}(M) + \Delta m_{expelled} + m_{L,exc.}}{m_{Solv.}} \quad . \quad (7)$$

Combination of equation (7) with equations (1) - (4) yields:

$$m''_{non-acc.}(M) = m'_{GS} - m_{PN} + \left[1 - \frac{w'(M)}{w''(M)}\right] \cdot m_{Solv.} \quad . \quad (8)$$

The use of GPC to measure concentrations of the various solutes enables determination of the dilution ratio $\frac{w'}{w''}$. The other mass quantities are measured by weighing. These data provide the amount of non-accessible liquid as a function of molecular weight.

To convert molecular weight M into a solute radius, we use the hydrodynamic volume of a solute, which has been well accepted as a size parameter. The following equations give experimentally-determined[15] relations between the molecular weights and the hydrodynamic radii of the solutes in water[16]:

$$r(Å) = 0.271 \cdot M^{0.498} \quad \text{Dextran} \quad (9)$$

$$r(Å) = 0.255 \cdot M^{0.517} \quad \text{Poly(ethylene glycol)} \quad (10)$$

$$r(Å) = 0.166 \cdot M^{0.573} \quad \text{Poly(ethylene oxide)} \quad (11)$$

Here M is the molecular weight corresponding to M_P, the peak volume in the distribution curve. If M_p is not stated by the supplier, the elution volume of polydisperse samples corresponding to M_n or M_w must be evaluated[8], using, for example, the Lansing-Kraemer distribution [8] or the less accurate estimate $M_P = \sqrt{M_W \cdot M_n}$.

The distribution coefficient K(r) as a function of solute radius r is the ratio of the accessible amount of imbibed liquid for a particular solute of radius r to the total amount of imbibed liquid:

$$K(r) = \frac{m_{Acc.}(r)}{m_{Total}} = \frac{V_{Acc.}(r)}{V_{Total}} \quad . \tag{12}$$

The accessible amount and the total amount of imbibed liquid are defined by the following equations:

$$m_{Acc.}(r) = m_{Total} - m_{Non-acc.}(r) \tag{13}$$

$$m_{Total} = \lim_{r \to \infty} m_{Non-acc.}(r) = m_{Non-acc.,\infty} \quad . \tag{14}$$

Combination of Eq. (12)-(14) yields:

$$K(r) = \frac{m_{Non-acc.,\infty} - m_{Non-acc}(r)}{m_{Non-acc,\infty}} \quad . \tag{15}$$

K(r) is the integral distribution coefficient, which is calculated from the experimentally-measured non-accessible amount of imbibed liquid (Eq.(8)). K(r) is given by an integral that is solely a function of solute radius r integrated over the entire pore-size range ($0 \le R \le R_{max}$). The following section discusses the differential distribution coefficient K(R,r) as a function of solute radius r and pore radius R.

Equation (8) represents the Solute-Exclusion (SE) curve which provides information about the quantity of non-accessible water within the gel as a function of probe-solute radius. Kuga[5] regarded Eq.(8) as the cumulative pore volume of the gel, but later[6] he states that the identification of the SE-curve with the pore-size distribution is not correct. This incorrect identification would mean that all the liquid existing in pores greater than the molecular size of a solute is available as accessible volume. Moreover, it would mean that the distribution coefficient for a solute of radius r, fitting into pores where $R \ge r$, is unity regardless of pore size. The latter statement is incorrect as long as the solute has a finite volume because of the excluded-volume effect (also known as the

Wall Effect), shown in Fig. 1.[16]. The Wall Effect requires information about partitioning of solutes between the outer solution phase and the gel phase as a function of solute size and pore size. This information is expressed by the differential distribution coefficient K(R,r). In the absence of any interaction between the solute and the polymer matrix of the gel (standard conditions of GPC), all solutes of any type give the same K(R,r)[17,18]. Casassa et al[19-21] developed a theory to represent the integral distribution coefficient for various pore geometries. This theory, based on the Brownian motion of a particle, has been verified for independently characterized porous materials, for example porous glasses. Fig. 2 shows the differential distribution coefficient as a function of r/R for three geometric cavities ; here r is the radius of the solute and R the radius of the cavity (pore). The three equations for the differential distribution coefficient are:

$$\text{Sphere:} \quad K(R,r) = \frac{6}{\pi^2} \sum_{m=1}^{\infty} \frac{1}{m^2} e^{-(m\pi \frac{r}{R})^2} \qquad (16)$$

$$\text{Cylinder:} \quad K(R,r) = 4 \sum_{m=1}^{\infty} \frac{1}{\beta_m^2} e^{-(\beta_m \frac{r}{R})^2} \qquad (17)$$

where β_m are the roots $J_o(\beta) = 0$ where J_o indicates a Bessel function of the first kind and zero order.

$$\text{Slab:} \quad K(R,r) = \frac{8}{\pi^2} \sum_{m=0}^{\infty} \frac{1}{(2m+1)^2} e^{-(\frac{(2m+1)\pi}{2} \frac{r}{R})^2} \qquad (18)$$

Haller[22] measured distribution coefficients for various controlled porous glasses (CPG) whose average pore diameters[23] ranged from 84 to 517Å. Comparison between the three theoretical curves and the experimental data suggests that the slab cavity is the best geometric pore shape for a reasonable representation of the experimental data. To our knowledge, these are the only experimental data using dextran probe solutes to measure distribution coefficients of porous materials with known pore-size distributions. Even though the slab cavity does not necessarily represent the porous structure of hydrogels,

it leads to the best representation of the experimental data. To calculate the distribution coefficient with cylindrical-shaped pores, the roots β_m of the Bessel-function of the first kind and order zero were taken from Carslaw and Jaeger[24]. The good agreement between experiment and theory supports the validity of the theoretical framework developed by Casassa.

The differential distribution coefficient K(R,r) is related to the pore-size distribution in the following way. Consider a group of pores of radii between R and R + dR with a total volume dV. Let $dV_{Acc.}(r)$ be the pore volume with pores of radii between R and R + dR accessible to a molecule of radius r. The amount of accessible volume for this group of pores is:

$$dV_{Acc.}(r) = K(R,r) \cdot dV \tag{19}$$

where K(R,r) is the differential distribution coefficient for solutes with radius r when the pore radius is R. The differential distribution coefficient is restricted to the region $0 \leq K(R,r) \leq 1$.

The differential pore-size distribution, denoted by f(R), is defined through:

$$\frac{dV}{V_{Total}} = f(R) \cdot dR \tag{20}$$

where $f(R) \cdot dR$ represents the fraction of the total pore volume that contains pores with radii between R and R + dR. Combination of equations (19) and (20) gives:

$$dV_{Acc.}(r) = K(R,r) \cdot f(R) \cdot V_{Total} \cdot dR \tag{21}$$

The total accessible volume for a solute molecule with radius r for all groups of pores is found from integration of equation (21):

$$\int_0^{V_{Acc.,\infty}} \frac{dV_{Acc.}(r)}{V_{Total}} = \int_0^{R_\infty} K(R,r) \cdot f(R) \cdot dR \tag{22}$$

Integration of the left side yields the integral distribution coefficient K(r) in accordance with Eq.(12):

$$K(r) = \frac{1}{V_{Total}} \int_0^{R_\infty} dV_{Acc.}(r) = \frac{V_{Acc.}(r)}{V_{Total}} \quad . \tag{23}$$

To obtain the differential pore-size distribution, the final equation for data reduction is:

$$K(r) = \int_0^{R_\infty} K(R,r) \cdot f(R) \cdot dR \quad . \tag{24}$$

The left side of Eq.(24) is the measured overall distribution coefficient as a function of molecular radius r. The right-hand side consists of the differential distribution coefficient as a function of r and R and the desired pore-size distribution f(R). The differential distribution coefficient K(R,r) is provided by the Casassa Model.

Solving integral equation (24) to obtain f(R) presents a serious problem. This equation is well-known as the inhomogeneous Fredholm equation of the first kind; it can only be solved numerically. We use the computer program CONTIN developed and maintained by Provencher[26-29] to calcuate pore-size distributions. It is called CONTIN because it is often applied to solving integral equations of the first kind for effectively CONTINuous distributions of diffusion coefficients, molecular weights, etc.[29]. Numerical solution of the Fredholm integral equation by inversion[30] induces additional mathematical instabilities creating a large (typically infinite) set of solutions f(R) that satisfy equation 24 within experimental error. These well-known instabilities are minimized by constraining the pore-size distribution to be the smoothest nonnegative distribution that is consistent with the experimental distribution coefficient K(r). The modular and clearly arranged structure of the computer program enables a user to incorporate additional theoretical models for particular applications not already included in the program. We included Eq.(18) in the subprogram USERK to account for the Wall Effect represented by the integral distribution coefficient K(R,r). Also, we changed the dimension spec-

ifications; we increased the number of quadrature grid points beyond 35 to obtain more accuracy. In some cases we used 250 grid points.

To verify the Brownian-Motion Model in conjunction with the solution of the Fredholm integral equation, we utilized experimentally-determined distribution coefficients K(r) of dextran solutes in various controlled porous glasses with independently known mean-pore diameters[22]. Calculation of pore-size distributions using the experimentally-determined distribution coefficients yields reasonable agreement of the average-pore size or mean-pore size with the CPG-data as shown in Table 1. Because the pore-size distributions of these controlled porous glasses are not available, a comparison of measured and calculated pore-size distributions is not possible.

Experimental Section

Synthesis of the acrylamide-based hydrogels is described by Baker et al.[31]. These hydrogels are able to swell to the order of hundreds of times their dry weight due to the hydrophilic nature of acrylamide. Incorporation of copolymer MAPTAC enlarges the swelling capacity due to an osmotic-pressure driving force allowing more water to enter the gel phase. To maintain electroneutrality, the Cl ions of the MAPTAC molecule are confined to the gel phase because of the quaternary amine groups imbedded in the gel network. Therefore, additional water migrates into the gel phase to dilute the concentration of the Cl ions. Hydrophilicity and osmotic pressure yield hydrogels that can immobilize large amounts of water or aqueous solution. However, these hydrogels display a weak structure, that is, they break easily under mechanical stress. Increasing %T and %C reinforces the polymer network; however, the ability of the gel to absorb water then decreases.

Gel compositions are shown in Table 2. Our goal is to isolate the effects of %C and %T on pore-size distribution. In our hydrogels the loweat %T was 15% and the lowest %C was 0.2%. Hydrogels with both low %T and %C are very fragile. Shifting %C and

%T to higher values increases the rigidity of the hydrogel but also yields hydrogels whose structure is insensitive to further changes in %C and %T.

Using one solution containing all solutes of a series requires a highly resolving chromatographic apparatus and essentially monodisperse polymer fractions to resolve each solute peak sufficiently for reasonable accuracy. Kuga's chromatograms show that individual solute peaks are close together; therefore, determination of solute concentrations leads to large analytical errors. To increase analytical accuracy, we split the all-solute solution into three or four subsolutions; each of these contains three solutes at most. Tables 3 and 4 show the solutes used in this work. These tables also show molecular weight, polydispersity and supplier. Tables 5 and 6 give the compositions of the solutions used for the MSE method.

Experiments for hydrogels with variable %T were performed with slightly polydisperse solutes. Determination of the dilution ratio in Eq. (8) has to be as accurate as possible because inaccurate measurements produce the largest random errors in the non-accessible water calculated from Eq. (8). For hydrogels varying in %C, more nearly monodisperse polymer fractions were used as shown in Table 6. These more nearly monodisperse fractions improve significantly the concentration measurements by producing a higher resolution of the peaks in the chromatogram.

Use of subsolutions to increase analytical accuracy induced new experimental difficulties. Contacting identical hydrogels with several solutions containing different solutes yields unequal swelling equilibria and thus diverse pore strucutres caused by different osmotic pressures. The pore-size distribution cannot be obtained correctly from combination of measured data from the various subsolutions. To circumvent this difficulty, it may be feasible to normalize the non-accessible water with the swelling capacity in equilibrium assuming a linear relationship between the swelling of a gel and its porous structure[33]. Another option is to increase the ionic strength of the surrounding solution by adding the salt sodium azide to the solutions to screen the effect of different osmotic

forces[34]. Toward that end, sodium azide is used in this work with a concentration 0.06519g NaN_3 per 1000g solution (0.001 M) to maintain the same degree of swelling of one class of hydrogels in equilibrium with each of the probe-solute-containing solutions.

Sodium azide also serves as an antibacterial agent for preventing the destruction of solutes (especially sucrose, raffinose and glucose[35]) by bacteria. In our initial experiments, we observed a degradation of our hydrogels over three months resulting in a steady increase of the swelling capacity[28]. Since the gel discs are cut from gel sheets, polymer strands are destroyed, leaving radicals on the gel discs. These radicals initiate the degradation in the gel in conjunction with dissolved oxygen and promote further break-up of polymer strands[36]. Because of its low ionization potential, the azide ion easily transfers an electron to the radical, saturating its electron shell; therefore, the azide ion inhibits decomposition of the hydrogel[36]. In the presence of sodium azide, hydrogels were stabilized; no change in swelling was observed over a long time.

To determine the dilution ratio in Eq. (8), it is necessary to conduct concentration measurements of the stock solutions and the corresponding equilibrated solutions. Since the solutions contain more than one probe solute, it is necessary to separate the solutes and subsequently to detect them. Probe solutes of one series differ only in molecular weight; Gel Permeation Chromatography (GPC) was used to separate the solutes as described in Reference 13.

The experimental procedure starts with weighing of gel samples to determine m'_{GS}. We used about 6 - 8 grams for each jar where gels and solution are placed to reach equilibrium. The jars are staight-sided, including a lid with a gasket for a tight seal. The tendency of polyacrylamide gel to adhere to the surfaces of the jars resulted in broken or damaged gel discs upon removal. Therefore, all jars were placed into a dichlorodimethyl silane - toluene solution for about 30 seconds to achieve hydrophobic glass surfaces of the jars. The jars were then thoroughly cleaned and rinsed with nanopure water.

The amount of stock solution added was about 1.4 times the weight of the swollen gel. This amount of solution was chosen to obtain a maximum decrease of the concentration of the small probe solutes of about 50% to guarantee a significant signal/noise ratio in the chromatogram. We used two jars for each gel/solution combination for determining experimental errors on the one hand and to minimize the number of jars on the other. The filled and closed jars were transferred to a constant-temperature bath purchased from Blue M Electric,Blue Island, IL 60406, Model MSB-3222 A-1. Constant temperature is maintained at 25°C.

For each class of gels, two jars contacted gel with pure water to monitor the effect of broken gel particles. The pure solvent was later filtered and analyzed by GPC to check the existence of any additional peak caused by dissolved gel particles. Diffusion jars were prepared to contact each class of gel with the largest probe solute of each series (Dextran 2.000.000, PEO 4.000.000). These diffusion jars were filled with three times the amount of gel and solution of the regular jars to modify the equilibration as little as possible. We sampled every second day the surrounding solution to measure the concentration as a function of time neccessary to determine the partitioning equilibrium of the probe solutes. These large polymers finished their migration after about 10 days; however, we terminated the experiment after 14 days.

After equilibrium was reached, the gel discs were separated from the equilibrated solutions, thoroughly washed to remove essentially all probe solutes and subsequently dried and weighed to determine m_{PN}. The equilibrated solutions were first filtered (Whatman filter paper no. 40, crystalline retention) to remove gel particles which would affect the chromatographic measurements. After filtering, the equilibrated solutions and the corresponding stock solutions were alternately chromatographed at least three times. Alternate measurements of stock solution and equilibrated solution were necessary to obtain accurate chromatographic results, because slight changes of the GPC-equipment (state of the column, temperature, state of the mobile phase) greatly affect the results.

Results and Discussion

Figures 3 and 4 show the solute-exclusion curves for the 20% and 30%-T hydrogels. The lower limit, a non-accessible volume of zero, can be confirmed experimentally. However, some data points lie in the negative range due to the limited accuracy of the measurements. This lower limit is independent of solute radius below 6Å; molecules with radii smaller than 6Å are able to enter the entire gel-pore structure. The upper limit representing the swelling capacity is experimentally determined by two different methods. The solid and dashed lines represent the weighed swelling capacities of the gels in equilibrium with the various probe-solute solutions. The data show the results of the mixed-SE method; data in the high-molecular-weight range (total exclusion) represent also the swelling capacity. Both methods show good agreement within experimental error. The data show that solutes with radii of 186Å or larger are totally excluded from both gels; however, between the lower and the upper limit, the exclusion behavior of both gels is different because of different pore structures. Generally, with increasing gel fragility, the data scatter increases due to breaking of the gel. Standard deviation of the non-accessible volume is about 25% for the 20% T gel, whereas the more rigid 30% T gel exhibits only 10% standard deviation.

Figs.5-7 show solute-exclusion curves for the 0.4, 0.8 and 1.2%C cross-linked hydrogels. The 1.2% gel, the tightest one, excludes solutes with radii of about 200Å, while the 0.4% gel, with the loosest network, accomodates molecules in its structure up to radii of only 160Å. Weighed swelling capacities in equilibrium with either dextran and PEO/PEG solutions agree better with increasing %C, again due to the increasing rigidity of the gel. No significant difference of the swelling capacities of the 1.2% gel was measured; the dashed line coincides with the solid line. The data fit (Fredholm) line is the curve calculated by CONTIN which gives the smoothest non-negative pore-size distribution.

Figs.6 and 7 show the calculated pore-size distribution for the hydrogels varying in %T and %C, respectively. The median represents pore radii with the highest probability;, the mean radius is the first moment of the distribution and the variance is the second mo-

ment. The tighter 30% T gel exhibits a pore-radius range to 300Å, whereas the 20%-T gel possesses pores with radii to 500Å. The hydrogels varying in %C are much tighter than the %T gels, although the %T content is only 15%. The 0.4% cross-linked gel possesses pores with maximum radii of 240Å; the 0.8% C and 1.2% C gels have pores with maximum pore radii of 200 and 180Å, respectively. The broadening of the distributions is represented by the variance; decreasing %C produces a looser network and therefore a broader distribution as indicated by a larger variance. Tables 7 and 8 give the modes, means and variances for all measured pore-size distributions.

Conclusions

For rational design of hydrogels, it is useful to know how the pore-size distribution depends on the hydrogel characterization commonly expressed by %C, %T and %comonomer. This work reports m measurements of pore-size distributions for acrylaamide-MAPTAC gels for the range %C from 0.2 to 1.2, %T from 15 to 30; %MAPTAC was constant at 3%. Measurements are based on the mixed-solute exclusion method using dextran or poly (ethylene-glycol/oxide) as probes. Mean pore sizes are in the range 67 to 168 Å. Mean pore sizes and variances decrease with rising %T and rising %C. The gels that are most dense (high %C and high %T) have appreciable numbers of very small pores (diameters of the order of 1 Å); as the gel becomes less dense, the frequency of such small pores becomes very low.

Acknowledgments

This work was supported by the Director, Office of Energy Research, Office of Basic Energy Sciences, Chemical Sciences Division of the U.S. Department of Energy under Contract Number DE-AC03-76SF00098 and by the National Institute of Health under Grant Number R01 GM 46788-01. Michael Kremer is grateful to the DAAD for financial support through a fellowship. The authors would like to thank Judy Lee, Jeannie Ahn, Helen Lam and Anthony Hui who performed some of the measurements.

References and Notes

(1) Mark-Bikales-Overberger-Menges, Encyclopedia of Polymer Sience and Engineering, Volume 6, Second Edition, **1986**, John Wiley & Sons pp.514-531

(2) Ratner, B.D.;Hoffman, A.S.; ACS Symposium Series, **1976**, 31, 1-37

(3) Sassi, A.P.; Blanch, H.W.; Prausnitz, J.M. in Polymer Applications for Biotechnology, Macromolecular Separation and Identification, edited by David S. Soane, Prentice Hall, Englewood Cliffs, New Jersey, **1992**, Chapter 8, 244-275

(4) Vashegani-Farahani, E.; Cooper, D.G.; Vera, J.H.; Weber, M.E. Chemical Engineering Science **1992**, 47(1), 31-40

(5) Kuga, S.;Journal of Chromatography, **1986**,206,449-461

(6) Kuga, S.; Journal of Chromatography Library, Volume 40 **1988**, Chapter 6

(7) Hooper, H.H.; Baker, J.; Blanch, H.W.; Prausnitz, J.M. Macromolecules, **1990**, 23, 1096

(8) Hagel, L; Journal of Chromatography Library, Volume 40 Chapter 5, **1988**

(9) Aggebrandt, Samuelson; Journal of Applied Polymer Science, **1964**,2,2801-2812

(10) Stone, J.E., Scallan, A.M.; Tappi, **1967**, 50(10), 496-501

(11) Stone, J.E., Scallan, A.M.; Cellulose Chemistry and Technology **1968**, 2, 343-358

(12) Stone, J.E., Treiber, E., Abrahamson, B.; Tappi, **1969**, 52(1), 108-110

(13) Kremer, M., Prausnitz, J.M.; Lawrence Berkeley Labaratory Report, LBL-32845, UC-401, **1992**

(14) ′ denotes all quantities which change during the experiments before contacting the probe solutions and the gel samples; ″ denotes all quantities at equilibrium.

(15) Measurements of intrinsic viscosity were used to determine hydrodynamic volumes. These volumes were used to calculate hydrodynamic radii for the solutes.

(16) Kubin, M., Vozka, S.; Journal of Polymer Science, Polymer Symposium **1980**, 68, 209-213

(17) Vilenchik, L.Z., Kurenbin, O.I., Zhmakina, T.P., Belen'kin, B.G. Doklady Akademii Nauk SSSR , **1980**, 250(2), 381-383

(18) Gorbunov, A.A., Solovyova, L.Ya.,Pasechnik, V.A. Journal of Chromatography, **1988**, 448, 307-332

(19) Casassa, E.F.; Journal of Polymer Science, Part B, **1967**, 5, 773

(20) Casassa, E.F., Tagami, Y.; Macromolecules, **1969**, 2, 14

(21) Casassa, E.F.; Macromolecules, **1976**, 9, 182

(22) Haller, W.; Macromolecules, **1977**, 10(1), 83-86

(23) The average-pore size of the controlled glasses (as determined by the mercury-intrusion technique) is defined as the pore diameter which was penetrated when half of the total volume available for mercury became filled[25].

(24) Carslaw, H.S.; Jaeger, J.C.; Conduction of Heat in Solids **1959**, Second Edition, Oxford at the Clarendon Press

(25) Haller, W.; Nature, **1965**, 206, 693-696

(26) Provencher, S.W.; Makromolekulare Chemie, **1979**, 180, 201-209

(27) Provencher, S.W.; Computer Physics Communications, **1982**, 27, 213-227

(28) Provencher, S.W.; Computer Physics Communications, **1982**, 27, 229-242

(29) Provencher, S.W.; Technical Report EMBL-DA07 (**1984**) CONTIN (Version 2) User's Manual

(30) Inversion means finding the desired pore-size distribution (which is under the integral) from the measured integral distribution coefficient K(r) .

(32) Baker, J.P.; Stephens, D.R.; Blanch, H.W.; Prausnitz, J.M. Macromolecules, **1992**, 25, 1955-1958

(33) Rößler, T.; unpublished research, UC Berkeley, Department of Chemical Engineering, **1992**

(34) As ionic strength increases, polyelectrolyte gels deswell due to screening of the fixed charges on the gel network. When not screened, these charges repel each other and contribute to the expansion of the network.

(35) Pothmann, E.; unpublished research, UC Berkeley, Department of Chemical Engineering, **1992**

(36) Kremer, M. (Lawrence Berkeley Laboratory Report, to be published)

Figure Captions

Figure 1 : The wall effect and the size-exclusion curve as a function of probe solute radius.

Figure 2 : Brownian Motion Model: Theoretical distribution coefficient as function of pore radius R and probe solute radius r.

Figure 3 : Size-exclusion curve for AAm MAPTAC hydrogel (20% T, 3% MAPTAC, 0.2%C). Data represents experiments performed with PEO/PEG and Dextran probe solutes. Data fit represents the fitted SE curve calculated and used by the computer program CONTIN to compute pore-size distributions, C swell (Dextran and PEO/PEG) is the swelling capacity of the used hydrogels determined by weighing measurements.

Figure 4 : Size-exclusion curve for AAm MAPTAC hydrogel (30% T, 3% MAPTAC, 0.2%C). Data represents experiments performed with PEO/PEG and Dextran probe solutes. Data fit represents the fitted SE curve calculated and used by the computer program CONTIN to compute pore-size distributions, C swell (Dextran and PEO/PEG) is the swelling capacity of the used hydrogels determined by weighing measurements.

Figure 5 : Size-exclusion curve for AAm MAPTAC hydrogel (15% T, 3% MAPTAC, 0.4%C). Data represents experiments performed with PEO/PEG and Dextran probe solutes. Data fit represents the fitted SE curve calculated and used by the computer program CONTIN to compute pore-size distributions, C swell (Dextran and PEO/PEG) is the swelling capacity of the used hydrogels determined by weighing measurements.

Figure 6 : Size-exclusion curve for AAm MAPTAC hydrogel (15% T, 3% MAPTAC, 0.8%C). Data represents experiments performed with PEO/PEG and Dextran probe solutes. Data fit represents the fitted SE curve calculated and used by the computer program CONTIN to compute pore-size distributions, C swell (Dextran and PEO/PEG) is the swelling capacity of the used hydrogels determined by weighing measurements.

Figure 7 : Size-exclusion curve for AAm MAPTAC hydrogel (15% T, 3% MAPTAC, 1.2%C). Data represents experiments performed with PEO/PEG and Dextran probe solutes. Data fit represents the fitted SE curve calculated and used by the computer program CONTIN to compute pore-size distributions, C swell (Dextran and PEO/PEG) is the swelling capacity of the used hydrogels determined by weighing measurements.

Figure 8 : Computed pore-size distributions usin CONTIN for AAm/MAPTAC hydrogel (0.2% C, 3% MAPTAC) varying in % T (20,30).

Figure 9 : Computed pore-size distributions usin CONTIN for AAm/MAPTAC hydrogel (15 % T, 3% MAPTAC) varying in % C (0.4, 0.8, 1.2).

Figure 1

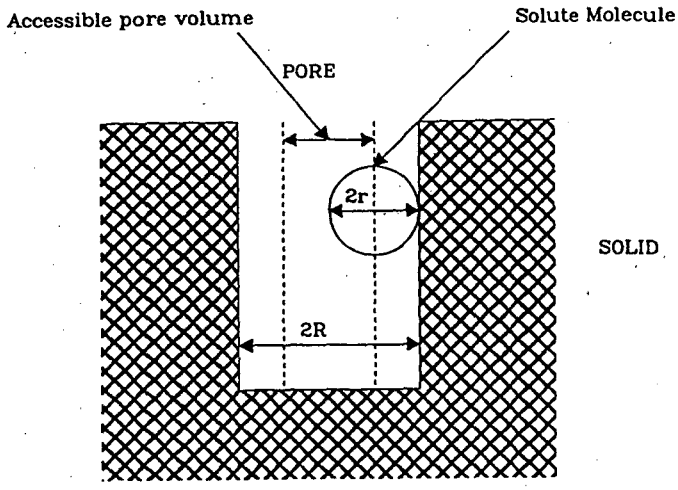
Accessible pore volume
Solute Molecule
PORE
2r
SOLID
2R

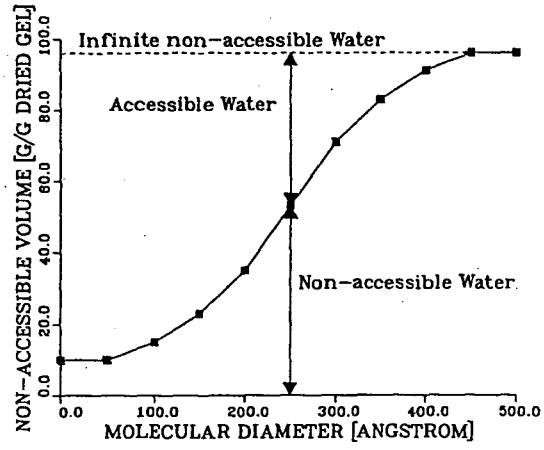
Infinite non-accessible Water
Accessible Water
Non-accessible Water
NON-ACCESSIBLE VOLUME [G/G DRIED GEL]
0.0
20.0
40.0
60.0
80.0
100.0
0.0
100.0
200.0
300.0
400.0
500.0
MOLECULAR DIAMETER [ANGSTROM]

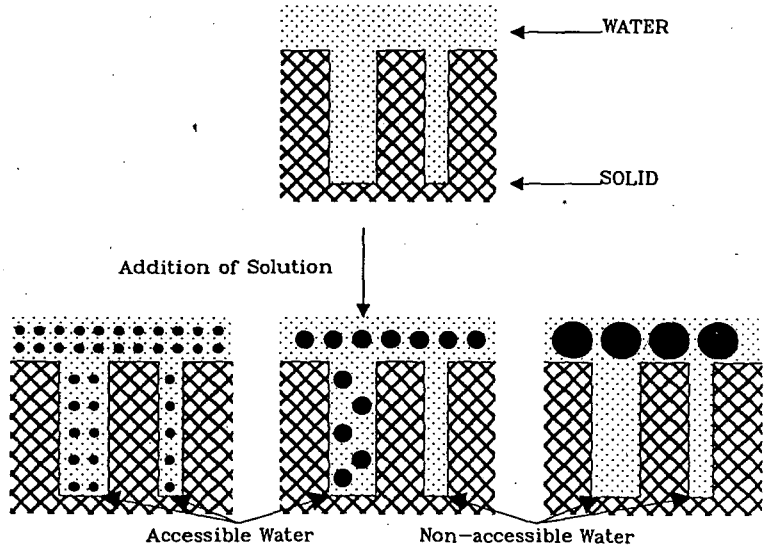
WATER
SOLID
Addition of Solution
Accessible Water
Non-accessible Water

Figure 2

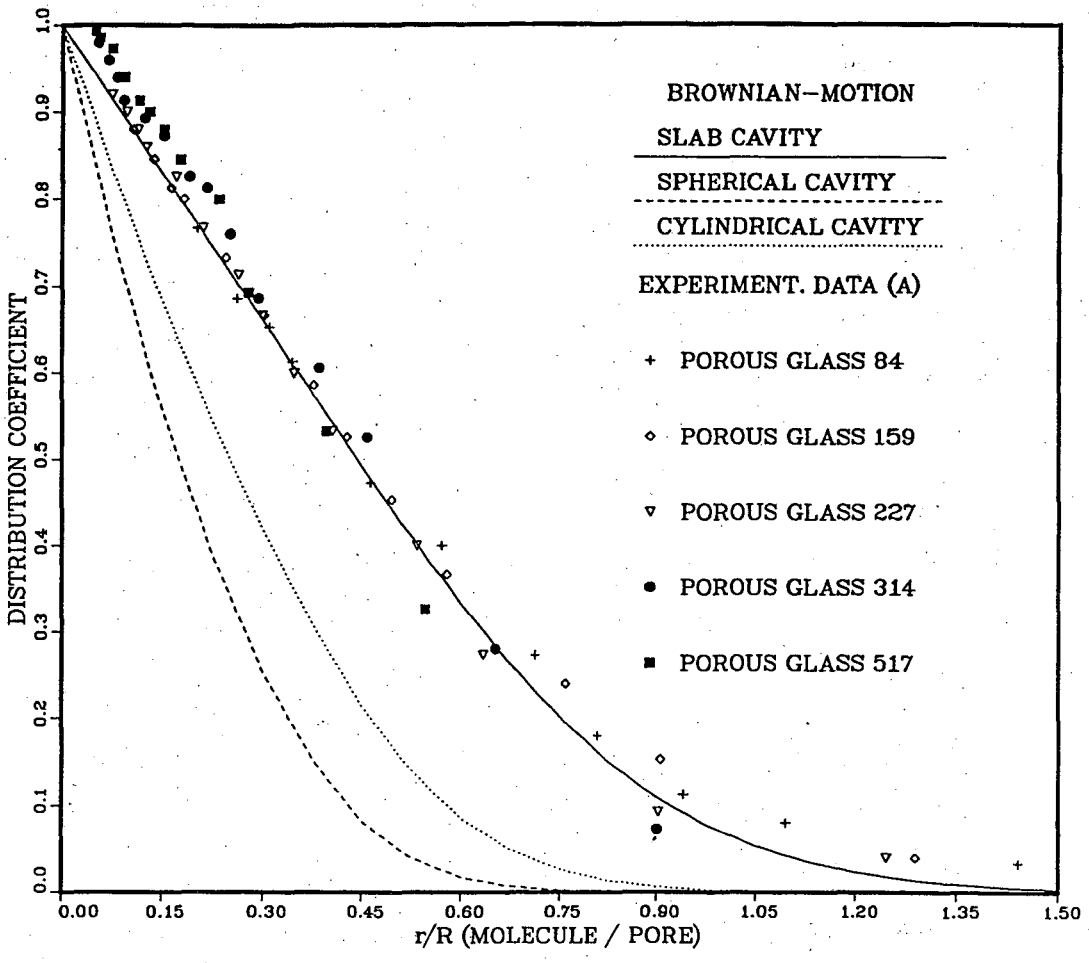
BROWNIAN–MOTION
SLAB CAVITY
SPHERICAL CAVITY
CYLINDRICAL CAVITY
EXPERIMENT. DATA (A)
POROUS GLASS 84
POROUS GLASS 159
POROUS GLASS 227
POROUS GLASS 314
POROUS GLASS 517
DISTRIBUTION COEFFICIENT
r/R (MOLECULE / PORE)
0.0
0.1
0.2
0.3
0.4
0.5
0.6
0.7
0.8
0.9
1.0
0.00
0.15
0.30
0.45
0.60
0.75
0.90
1.05
1.20
1.35
1.50

Figure 3

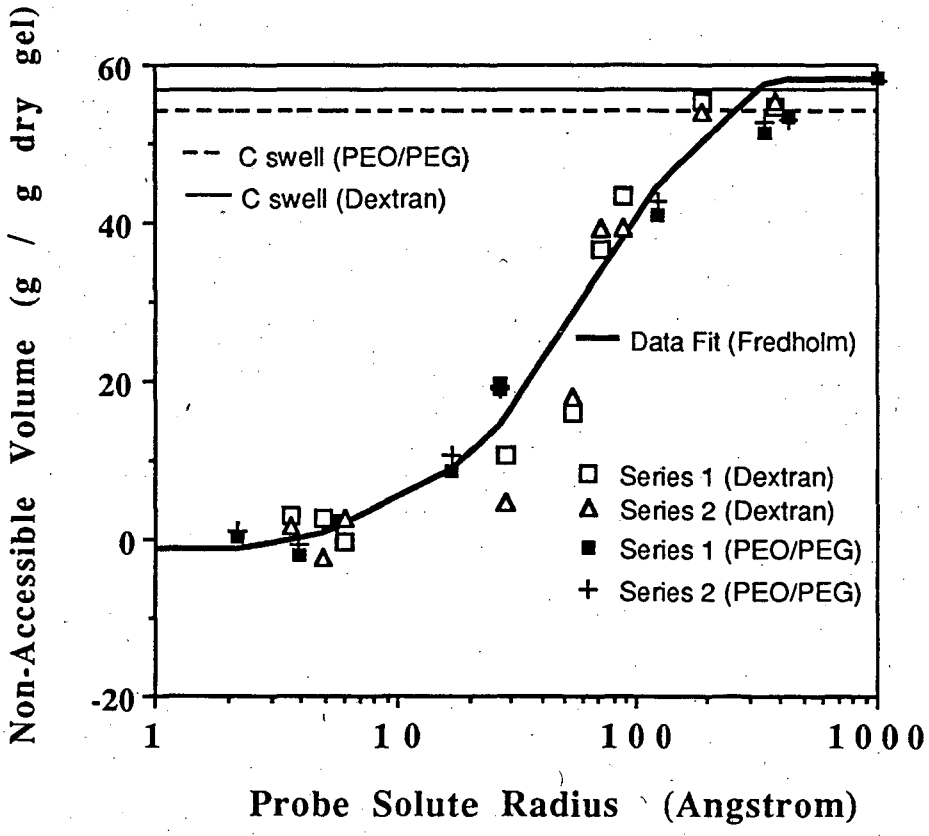
Non-Accessible Volume (g / g dry gel)
60
40
20
0
-20
1
10
100
1000
Probe Solute Radius (Angstrom)
C swell (PEO/PEG)
C swell (Dextran)
Data Fit (Fredholm)
Series 1 (Dextran)
Series 2 (Dextran)
Series 1 (PEO/PEG)
Series 2 (PEO/PEG)

Figure 4

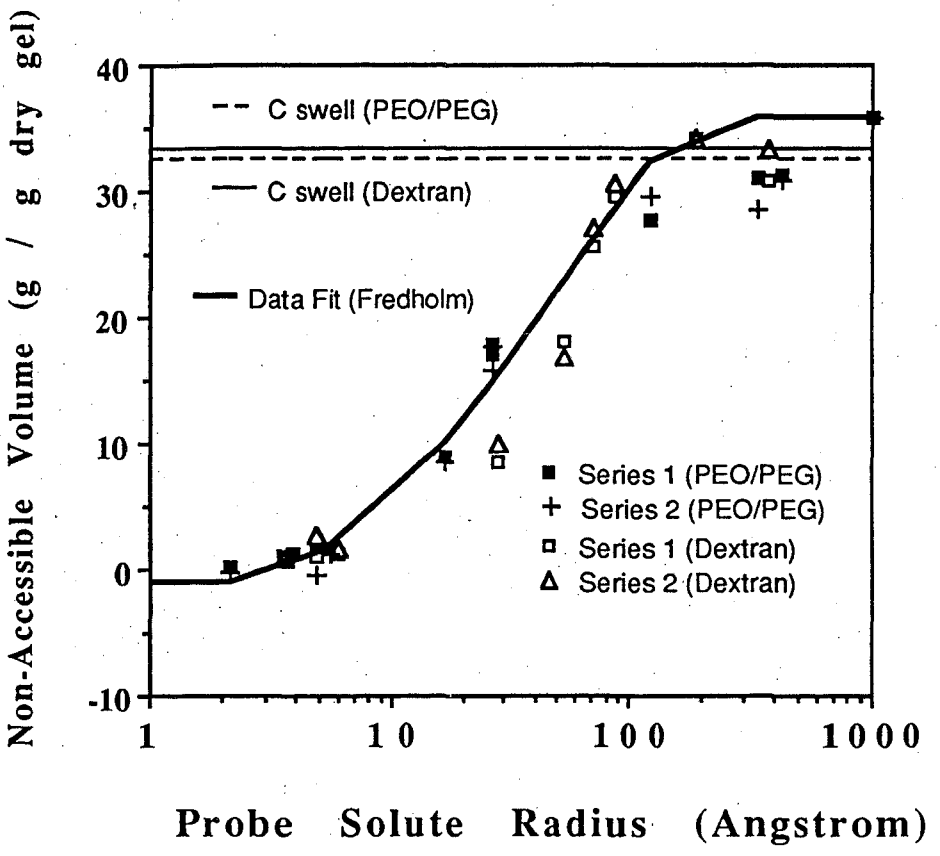
Non-Accessible Volume (g / g dry gel)
40
30
20
10
0
-10
1
10
100
1000
Probe Solute Radius (Angstrom)
C swell (PEO/PEG)
C swell (Dextran)
Data Fit (Fredholm)
Series 1 (PEO/PEG)
Series 2 (PEO/PEG)
Series 1 (Dextran)
Series 2 (Dextran)

Figure 5

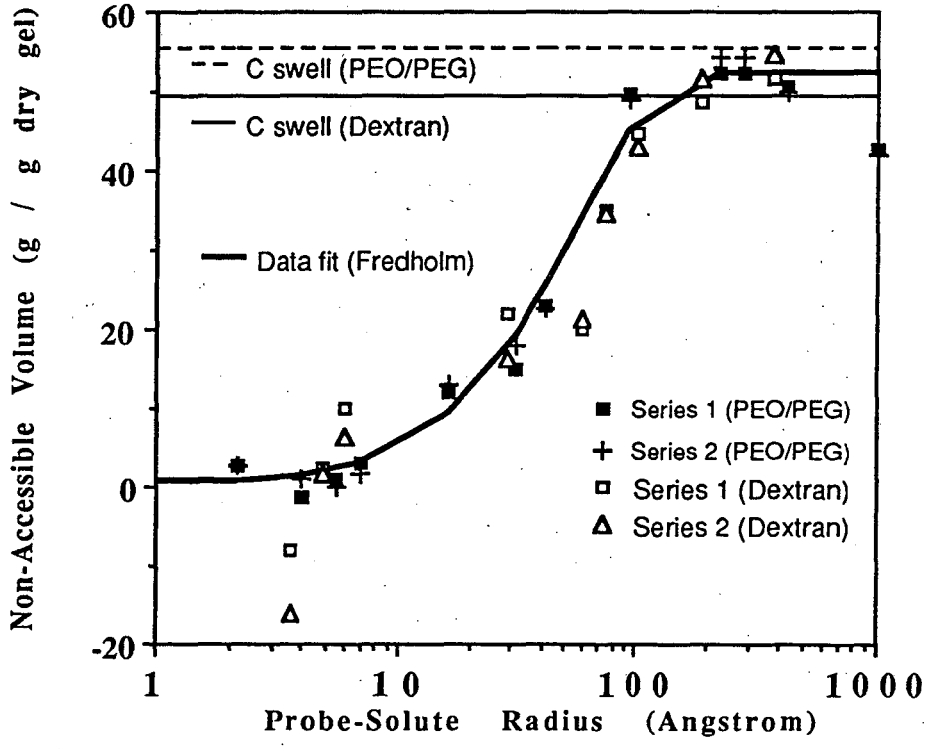
60
40
20
0
-20
1
10
100
1000
Non-Accessible Volume (g / g dry gel)
Probe-Solute Radius (Angstrom)
C swell (PEO/PEG)
C swell (Dextran)
Data fit (Fredholm)
Series 1 (PEO/PEG)
Series 2 (PEO/PEG)
Series 1 (Dextran)
Series 2 (Dextran)

Figure 6

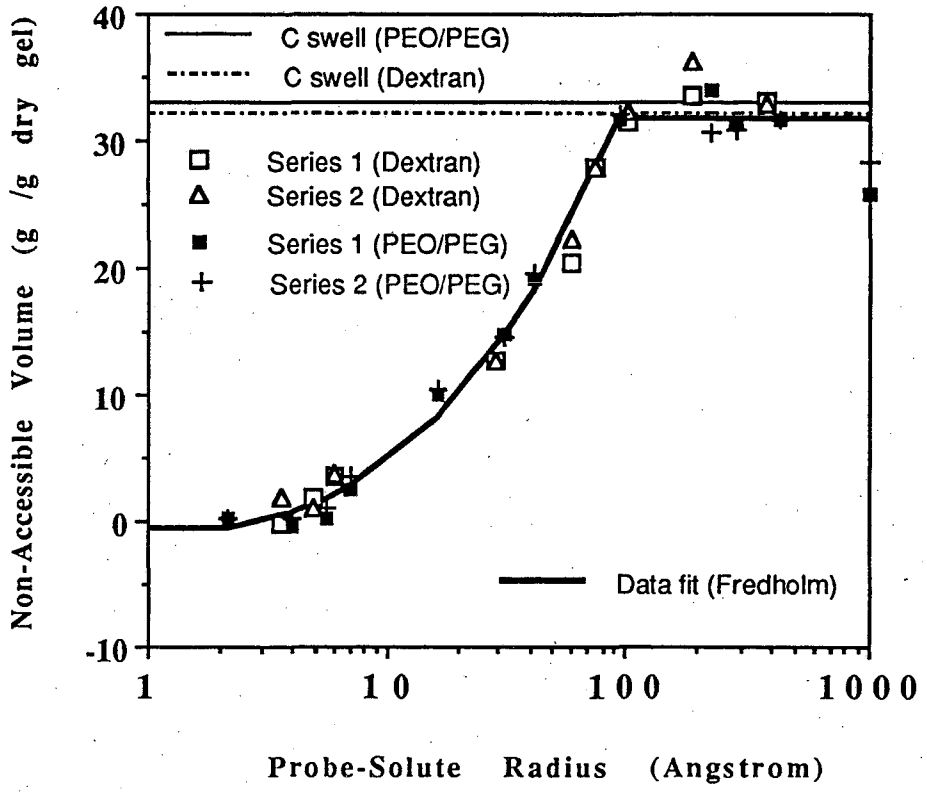
C swell (PEO/PEG)
C swell (Dextran)
Series 1 (Dextran)
Series 2 (Dextran)
Series 1 (PEO/PEG)
Series 2 (PEO/PEG)
Data fit (Fredholm)
Non-Accessible Volume (g /g dry gel)
Probe-Solute Radius (Angstrom)
40
30
20
10
0
-10
1
10
100
1000

Figure 7

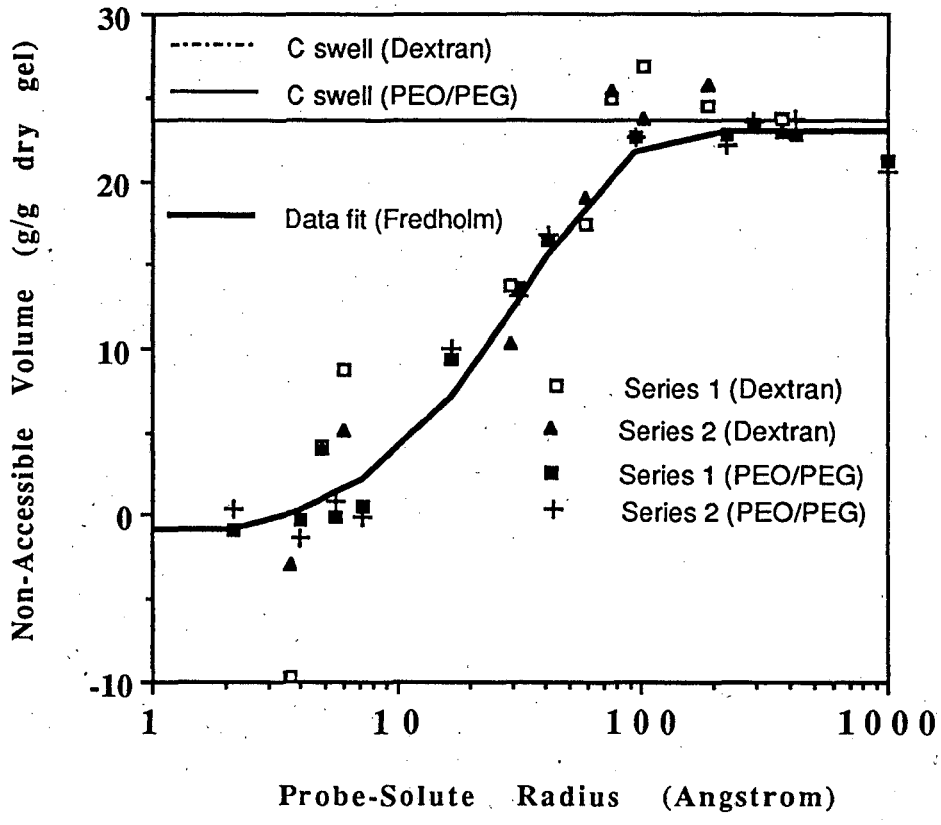
C swell (Dextran)
C swell (PEO/PEG)
Data fit (Fredholm)
Series 1 (Dextran)
Series 2 (Dextran)
Series 1 (PEO/PEG)
Series 2 (PEO/PEG)
Non-Accessible Volume (g/g dry gel)
Probe-Solute Radius (Angstrom)
30
20
10
0
-10
1
10
100
1000

Figure 8

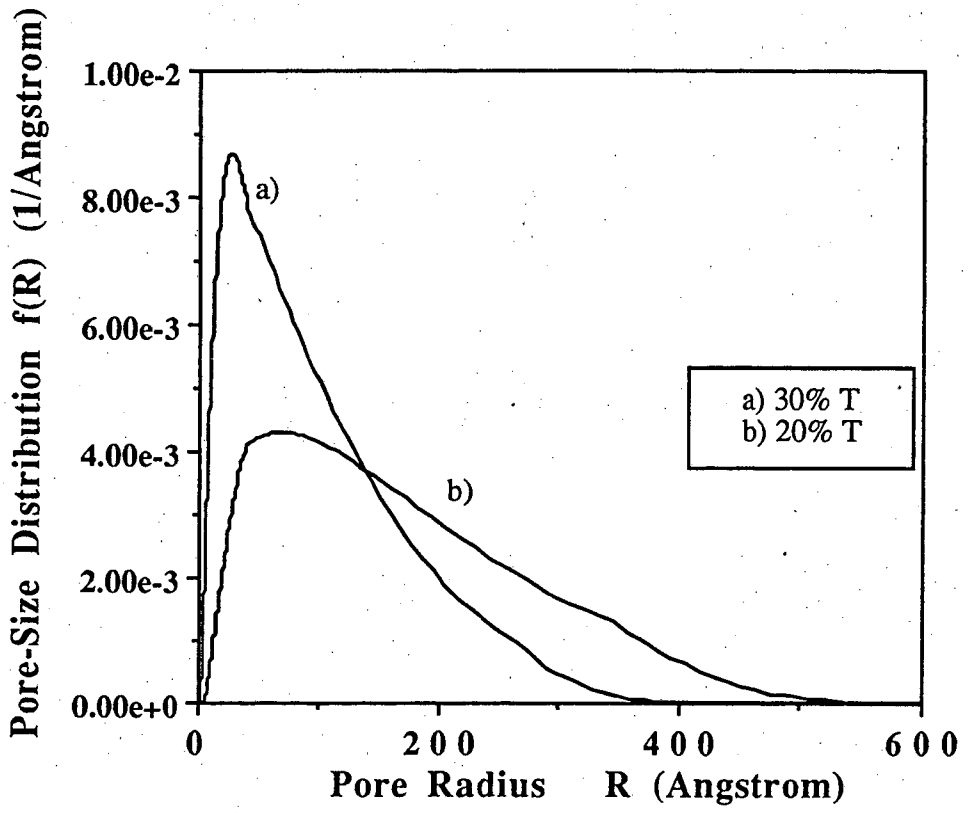
Pore-Size Distribution f(R) (1/Angstrom)
1.00e-2
8.00e-3
6.00e-3
4.00e-3
2.00e-3
0.00e+0
a)
b)
a) 30% T
b) 20% T
0
200
400
600
Pore Radius R (Angstrom)

Figure 9

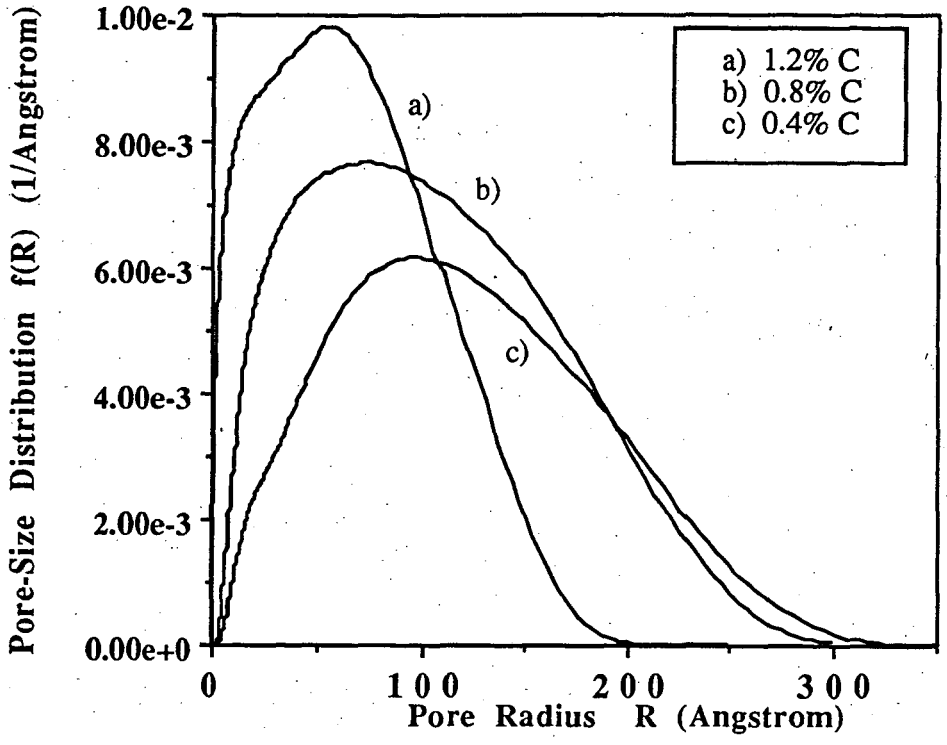
Pore-Size Distribution f(R) (1/Angstrom)
1.00e-2
8.00e-3
6.00e-3
4.00e-3
2.00e-3
0.00e+0
0
100
200
300
Pore Radius R (Angstrom)
a) 1.2% C
b) 0.8% C
c) 0.4% C
a)
b)
c)

Porous Glass Mean Diameter (A)	84	227	314	517
Calculated Mean Diameter (A)	90	222	312	470
Deviation (%)	7.1	2.25	0.6	10.0

Table 1:Comparison of experimentally-determined mean-pore diameters of controlled porous glasses and calculated mean-pore diameter using Brownian Motion model in conjunction with the solution of the Fredholm integral equation

	Variation %T				Variation %C		
%MAPTAC	3%				3%		
% C	0.2%				0.4%	0.8%	1.2%
% T	15%	20%	25%	30%	15%		

Table 2: Composition of AAm/MAPTAC hydrogels used in this work.

PEG/PEO		Dextran/Oligosaccharides	
M_W Fraction	Supplier	M_W Fraction	Supplier
EG (M_W=62)	Fischer	Glucose (M_W=180)	Aldrich
PEG 200	Union Carbide	Sucrose (M_W=342)	Fisher
PEG 300		Raffinose (M_W=504)	
PEG 400		11,000	Sigma
PEG 3350		2,000,000	
PEG 8000		70,000	Fluka
PEO 100,000	Aldrich	110,000	
PEO 600,000		40,000	Pharmacia
PEO 900,000		500,000	
PEO 4,000,000			

Table 3: Polydisperse PEO/PEG and Dextran/Oligosaccharide probe solutes used for investigation of AAM/MAPTAC hydrogels varying in %T. Polydispersity ranges from approximateley 1.4 to 2.8.

Solute	Weight Average (GPC) Mw	Weight Average (Light Scatter.) Mw	Number Average (GPC) Mn	Peak Average (GPC) Mp	Mw/Mn	Supplier
P E O 4.000.000	N/A	N/A	N/A	N/A	N/A	Aldrich Chem. Co.
P E O 1,000,000	832,000	888,600	876,400	881,500	1.06	Scientific Polymer
P E O 500.000	444,900	457,000	432,300	447,300	1.03	
P E O 200.000	305,400	299,300	283,400	293,000	1.08	
P E O 60.000	62,600	66,600	61,400	64,400	1.03	
P E G 20.000	19,700		14,700	19,000	1.34	
P E G 10.000	10,900		9,200	10,900	1.19	
P E G 3.000	3,070		2,890	3,140	1.06	
P E G 600	629		574	625	1.10	
P E G 450	420		370	400	1.14	
P E G 200	229		206	210	1.11	

Solute	Weight Average (GPC) Mw	Number Average (GPC) Mn	Mw/Mn	Supplier
Dextran 12,000	11,600	8,110	1.43	Fluka
Dextran 50,000	48,600	35,600	1.36	
Dextran 80,000	80,900	55,000	1.47	
Dextran 150,000	147,600	100,300	1.47	
Dextran 670,000	667,800	332,800	2.00	
Dextran 2,000,000	N/A	N/A	N/A	Sigma
Glucose			1.00	Aldrich
Sucrose			1.00	Fischer
Raffinose			1.00	

Table 4: Monodisperse probe solutes used for investigations of AAm/MAPTAC hydrogels varying in %C

PEG/PEO			Dextran		
Solution	Fraction	w' [wt%]	Solution	Fraction	w' [wt%]
P1	200	0.80	D1	110,000	0.15
	100,000	0.25		11,000	0.15
P2	300	0.70		Sucrose	0.06
	8,000	0.40	D2	500,000	0.15
	600,000	0.25		40,000	0.15
P3	400	0.70		Glucose	0.06
	8,000	0.40	D3	2,000,000	0.16
	900,000	0.25		70,000	0.20
P4	EG	0.10		Raffinose	0.06
	3,350	0.40			
	4,000,000	0.16			

Table 5: Compositions of stock solutions used for investigations of AAm/MAPTAC hydrogels varying in %T

PEO/PEG			Dextran		
Solution	MW	Weight percent	Solution	MW	Weight Percent
P1	E G 3,000 200,000	1.0 0.4 0.3	D1	Raffinose 12,000 150,000	0.06 0.1 0.2
P2	200 10,000 500,000	0.8 0.5 0.3	D2	Glucose 50,000 670,000	0.06 0.15 0.2
P3	450 20,000 1,000,000	0.8 0.6 0.25	D3	Sucrose 80,000	0.06 0.2
P4	600 60,000 4,000,000	0.7 0.4 0.2	D4	2,000,000	0.2

Table 6: Compositions of stock solutions used for investigations of AAm/MAPTAC hydrogels varying %C

	Mode [A]	Mean [A]	Variance [A^2]
30% T	27.9	100.1	16555
20% T	72.9	168.8	41314

Table 7: Mode, mean and variance for pore-size distributions of AAm/MAPTAC hydrogels varying in %T.

	Mode [A]	Mean [A]	Variance [A^2]
0.4% C	99.5	124.8	20514
0.8% C	55.7	92.0	12109
1.2% C	54.4	67.8	6923

Table 8: Mode, mean and variance for pore-size distribution of AAm/MAPTAC hydrogels varying in %C.

LAWRENCE BERKELEY LABORATORY
UNIVERSITY OF CALIFORNIA
TECHNICAL INFORMATION DEPARTMENT
BERKELEY, CALIFORNIA 94720